Macromolecules

pubs.acs.org/Macromolecules Article

Importance of Viscosity Control for Recyclable Reinforced Thermoplastic Composites

Gijs W. de Kort,* Sarah Saidi, Daniel Hermida-Merino, Nils Leoné, Varun Srinivas, Sanjay Rastogi, and Carolus H. R. M. Wilsens*

Cite This: *Macromolecules* 2020, 53, 6690–6702 Read Online

ACCESS | Metrics & More | Article Recommendations | Supporting Information

ABSTRACT: Thermoplastic composites consisting of a liquid crystalline polymer (LCP) and poly(lactide) (PLA) have the potential to combine good mechanical performance with recyclability and are therefore interesting as strong and sustainable composite materials. The viscoelastic behavior of both the LCP and the PLA is of great importance for the performance of these composites, as they determine the LCP morphology in the composite and play a crucial role in preventing the loss of mechanical performance upon recycling. Though the effect of the matrix viscosity is well-documented in literature, well-controlled systems where the LCP viscosity is tailored are not reported. Therefore, four LCPs, with the same chemical backbone but different molecular weights, are used to produce reinforced LCP-PLA composites. The differences in viscosity of the LCPs and viscosity ratio between the dispersed phase and the matrix of the blends are evident in the resultant composite morphology: in all cases fibrils are formed; however, the diameter increases considerably as the viscosity ratio increases for the higher molar mass LCPs. The fibril diameter ranges from several hundred nanometer to a few micrometer. A typical layered structure in the injection molded composites is observed, where the layer-thickness is influenced by the LCP viscosity. The LCPs are found to effectively reinforce the PLLA matrix, increasing the Young's modulus by 60% and the maximum stress by 40% for the composite containing 30 wt % of the most viscous LCP. Remarkably, this did not result in an increase in brittleness, effectively increasing the toughness of the composite compared to pure PLLA. The feasible reprocessability of this composite is confirmed, by subjecting it to three reprocessing cycles. The relaxation of the LCPs orientation upon heating is measured via in situ WAXD. We compare the relaxation in an amorphous PLA matrix and in a semicrystalline PLLA matrix with that of the pure LCPs. The matrix viscosity is found to strongly influence the relaxation. For example, in a low viscous amorphous matrix relaxation of the LCP fibrils into droplets dominates the process, whereas a semicrystalline matrix helps in maintaining the fibril morphology and intermolecular orientation of the LCP. In the latter case, the LCPs relax via contraction and coalescence of the polydomain texture and maintains a significant degree of orientation until the PLLA crystals melt and the matrix viscosity decreases. The insights gained in this study on the role of the LCP viscosity on the morphology and performance of thermoplastic composites, as well as the relaxation of LCPs in a matrix, will aid progression toward sustainable and reprocessable LCP reinforced thermoplastic composites.

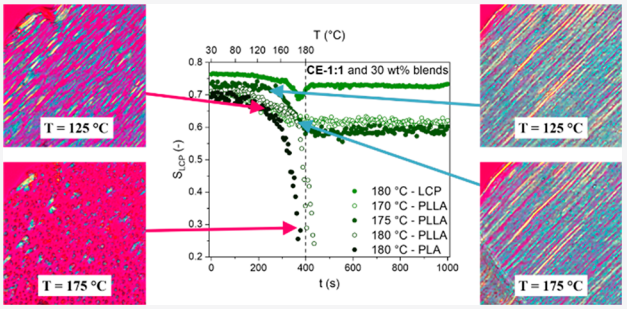

INTRODUCTION

Fiber-reinforced composites are a versatile class of materials, combining excellent mechanical properties with low density. These materials contribute to a more sustainable future, as their high specific properties allow, for example, weight saving and higher fuel efficiency in the transportation sector and novel structural components in construction.[1] However, at the end of their use, following failure of the composite, these materials are typically less sustainable as their recycling proves challenging.[2−4] The most common recycling strategies are mechanical recycling and fiber recovery. In mechanical recycling, the composite is ground and reprocessed. This process breaks and damages the reinforcing fibers, resulting in a decreased performance as the performance of the composite depends strongly on length and diameter of the reinforcing phase.[5−8] Fiber recovery involves removal of the matrix phase, *e.g.*, using a harmful solvent or via pyrolysis, although this process is generally resource intensive and the performance of the recovered fibers is not always comparable to the original fibers.[9,10]

Thermoplastic reinforced composites, such as composites based on liquid crystalline polymers (LCPs) and poly(lactide) (PLA), can provide a solution to this issue. These materials

Received: December 19, 2019
Revised: May 14, 2020
Published: July 30, 2020

https://dx.doi.org/10.1021/acs.macromol.9b02689
Macromolecules 2020, 53, 6690–6702

provide good mechanical performance, comparable to short glass fiber-reinforced composites, while being compatible with thermomechanical recycling.[11−13] In thermoplastic composites, both the reinforcing phase and the matrix phase are melt-processable, where the mechanical performance depends on the morphology of the dispersed phase (length, diameter, and distribution) formed during melt processing, similar to the fiber morphology dependency in regular fiber-reinforced systems.[14,15] For an LCP-PLA composite, we have demonstrated that the morphology and mechanical performance remain constant irrespective of the number of reprocessing cycles, given that the viscosity of the dispersed LCP phase remains lower than that of the PLA matrix (i.e., viscosity ratio < 1).[16]

Thermotropic LCP's are melt processable and are known for their excellent mechanical properties and low viscosity.[17,18] Both these properties stem from the rigid nature of the polymer backbone, allowing the LCP chains to be oriented on a molecular level by flow. This makes these materials highly suitable to serve as the reinforcing phase in thermoplastic composites: as the LCP droplets are deformed by the thermoplastic matrix in a flow field, elongated fibrils are formed with the LCP chains molecularly oriented along the fibril/flow direction. This results in the production of reinforced composites, given that this fibrillar LCP morphology can be maintained upon cooling. The morphology and chain orientation of the LCP are key parameters for the performance of LCP-reinforced composites.[13] Therefore, the mechanical performance is strongly governed by the processing conditions and, more importantly, the viscoelastic properties of both of the blend constituents.

The high processing temperatures (>300 °C) of commercial thermotropic LCPs and the lack of control over the viscosity of these materials limit their use in thermoplastic composite applications. The former hinders their use (and reuse) as reinforcing components in many thermoplastic matrices which generally suffer from a lower thermal stability, whereas the latter generally results in a high viscosity ratio for the blend ($\lambda > 1$, due to the high T_m of the LCP), which hinders the formation of the required fibrillar morphology. In general, the influence of the viscosity ratio on the blend morphology has been well studied. However, for LCPs in a thermoplastic matrix the emphasis has been on changing the matrix.[19,20] Due to their complex viscoelastic behavior, an approach based on altering the LCPs viscosity could provide valuable insight; however, these are scarce in literature as the molar mass is not easily controlled via typical acidolysis polycondensation. Recently, we have reported a route to obtain thermotropic LCPs with good mechanical performance, a low processing temperature and a tunable molecular weight, based on a thermal ring-opening addition reaction between carboxylic acid terminated LCP polymers and bis(2-oxazolines).[21] In this study, we make use of these LCPs to generate LCP-PLA composites and to investigate the effect of the LCP viscosity on the composite morphology and performance. The relaxation of the blends upon heating and the effect of the matrix phase are investigated via in situ wide-angle X-ray diffraction combined with polarized optical microscopy.

EXPERIMENTAL SECTION

Materials. The semicrystalline poly(L-lactide) (PLLA) grade was purchased from Total Corbion (Purapol L130) and the amorphous PLA grade was obtained from NatureWorks (Ingeo Biopolymer 6302D). The used LCPs were produced in house. The synthesis of the liquid crystalline prepolymer (**LCPP**) via acidolysis polycondensation and the production of the chain extended LCPs via reactive extrusion is reported in detail elsewhere.[21]

Preparation and Processing of PLA-LCP Blends. The PLA pellets, PLLA pellets, and previously produced LCPs were dried overnight (*in vacuo*, 60 °C) prior to use. Mixtures with containing 30 wt % LCP of the different LCPs and PLLA/PLA were prepared and fed in a preheated DSM Xplore twin-screw microextruder with a barrel size of 5 mL for extrusion. The recycle channel allows control over the residence time, and a valve can be switched to expel the material from the barrel. The materials were mixed for 3 min at 190 °C and 100 rpm. After extrusion, the samples were either processed directly into melt-drawn filaments or transferred into a preheated barrel and injection molded into tensile bars. Melt-drawn filaments were prepared using a slit die mounted at the extruder outlet (0.5 × 3 mm, produced by DSM Xplore) and a winder (Dienes SD-type). The tapes were drawn and cooled in air. A DSM Xplore IM 5.5 micro injection molder was used to produce tensile bars (2 × 4 × 70 mm, with a gage length of 25 mm). The barrel temperature was set to 190 °C, while the mold temperature was set to 25 °C. An injection pressure of 8 bar was used for all samples. The same processing conditions were used to reprocess the **CE-1:1**-PLLA composite thrice. The tensile bars were cut into pieces in between the processing cycles.

Material Characterization. The molecular weight distributions of the liquid crystalline prepolymer and the chain extended LCPs were determined via gel permeation chromatography (GPC) using a PSS SECcurity GPC system with Agilent 1260 Infinity instrument technology. The system is equipped with two PFG combination medium microcolumns with 7 μm particle size (4.6 × 250 mm, separation range 100−1.000.000 Da), a PFG combination medium precolumn with 7 μm particle size (4.6 × 30 mm), and a Refractive Index detector (RI). Distilled 1,1,1,3,3,3-hexafluoroisopropanol (HFIP) containing 0.019% sodium trifluoroacetate was used as a mobile phase at 40 °C, with a 0.3 mL min^{-1} flow rate. The obtained molecular weight distributions are relative with respect to poly(methyl methacrylate) standards obtained from PSS. Samples were prepared via dissolution of approximately 6 mg of LCP in 1.5 mL HFIP. The samples were shaken overnight and subsequently filtered over a 0.2 μm PTFE syringe filter prior to injection.

The viscoelastic behavior of the PLLA, PLA, and the LCPs was determined in a MCR 702 TwinDrive rheometer (Anton Paar) with a parallel plate geometry (diameter of 12 mm, gap of 0.7 mm). The PLLA samples were loaded at 190 °C and kept isothermal for 3 min to erase mechanical and thermal history. Subsequently, the samples were either heated or cooled at a rate of 5 °C min^{-1} to the measurement temperature and subjected to a frequency sweep with a strain of 0.5%. The LCPs were subjected to the same procedure with the exception that the samples were kept isothermal at 190 °C for 10 min.

The microstructure of the LCP-P(L)LA composites was evaluated via polarized optical microscopy, 2D-SAXS analysis, and SEM analysis. The injection molded bars were cut into thin slices (thickness of 1.0 and 2.5 μm, respectively) along the injection direction with a Leica EM UC7 ultramicrotome. These samples were studied via polarized optical microscopy (POM) using an Olympus BX53 Microscope (5 or 50 times magnification) equipped with an Olympus DP26 camera and a 530 nm retardation plate. To study the changes in morphology upon heating, slices with a thickness of 1.0 μm were cut along the drawing direction and Linkam HFSX350 temperature controlled stage was mounted on the microscope. The slices were placed between two glass plates and heated at a rate of 30 °C min^{-1} to 180 °C, while their morphology was monitored. Two-dimensional (2D) small-angle X-ray scattering (SAXS) analysis was performed on the LCP-PLLA injection-molded bars. A SAXSLAB Ganesha diffractometer was used with a sample-to-detector distance of 1076.3 mm, using Cu Kα radiation (λ = 1.5406 Å) and silver behenate (d001 = 58.380 Å) as a calibrant. Scanning electron microscopy (SEM) imaging was done on the fracture surfaces of the

https://dx.doi.org/10.1021/acs.macromol.9b02689
Macromolecules 2020, 53, 6690−6702

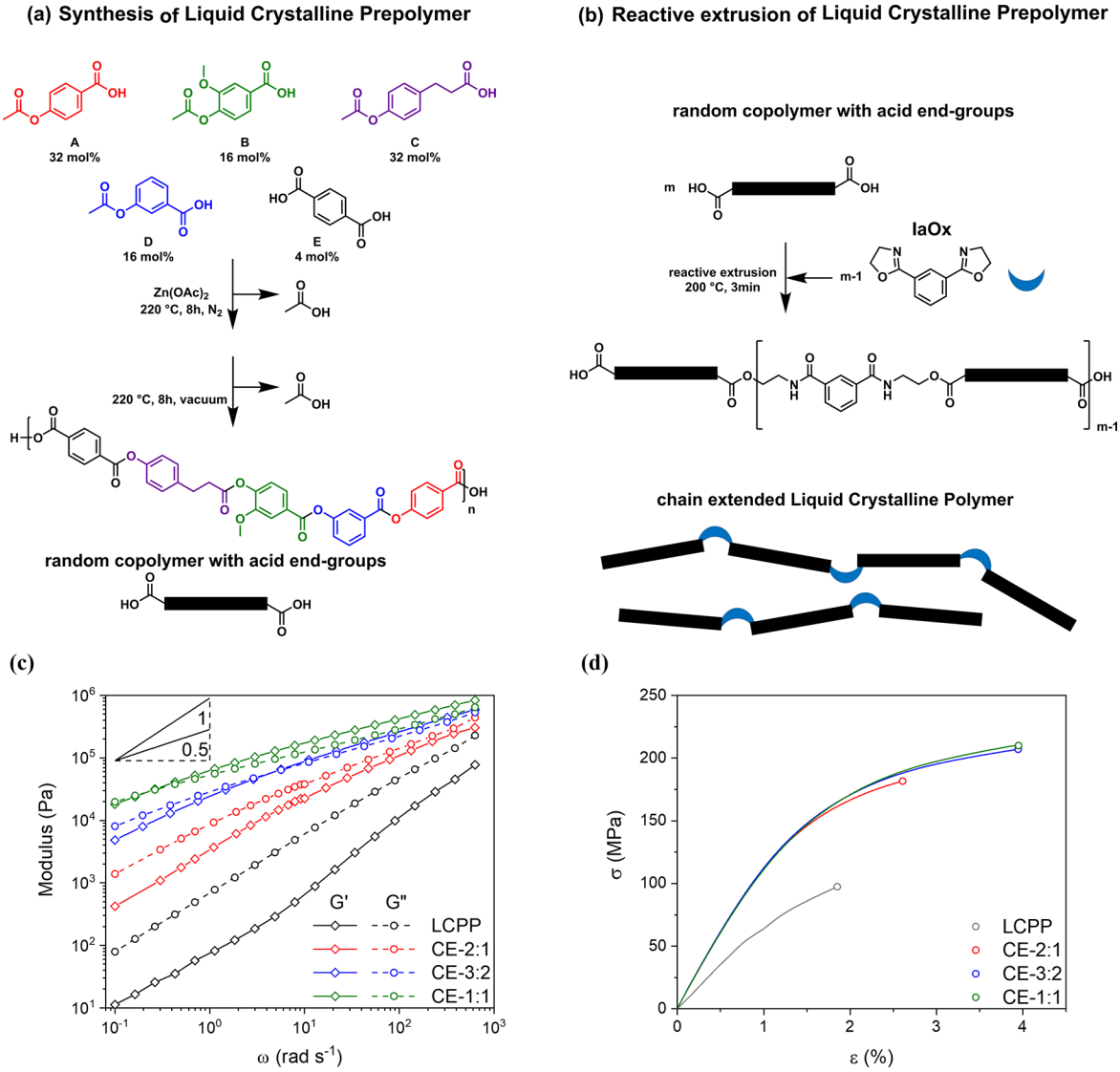

Figure 1. (a) Outline of the monomers and conditions used during the synthesis of the liquid crystalline prepolymer. (b) Outline of the reagents and conditions used in chain extension of the liquid crystalline prepolymer. (c) Storage and loss modulus as a function of angular frequency of LCPP and chain extended LCPs, measured at 150 °C in the linear viscoelastic regime. The lines in the top left corner mark slopes of 1 and 0.5, respectively. (d) Characteristic stress−strain curves of injection-molded bars, at room temperature, comparing LCPP and the chain-extended LCPs obtained by reactive extrusion. All figures are reproduced with permission.[21]

LCP-PLLA composites using a Philips X30 microscope at an acceleration voltage of 15 kV and a magnification of 15000×. The fracture surfaces were created by breaking samples cooled in liquid nitrogen, which were subsequently mounted and plasma-coated with a thin layer of gold prior to analysis.

The mechanical properties of the injection molded LCPs were assessed under tension. Measurement were performed on a Zwick Z100. Samples were subjected to a constant deformation rate of 5 mm min^{-1}, at room temperature.

Wide-angle X-ray diffraction (WAXD) measurements (wavelength, λ = 0.104 nm) were carried out at the European Synchrotron Radiation Facility (ESRF), the DUBBLE beamline (BM26B, Grenoble, France). The DUBBLE beamline is optimized for polymer science as is reported by Bras et al.[22] and Portale et al.[23] WAXD patterns, with an exposure time of 5 s, were collected using a Frelon detector (2048 × 2048 pixels of 48.8 × 48.8 μm) placed at a distance of 0.18 m. The data were normalized for synchrotron beam fluctuations using an ionization chamber placed before the sample. Furthermore, a correction for the sample absorption was performed using a photodiode located at the beamstop before the background contribution was subtracted. The wavenumber q = 4π sin θ/λ, with θ being half of the scattering angle for WAXD experiments scale calibration, has been achieved by α-Al2O3 (alumina). The samples were loaded into a Linkam CSS 450 shear cell, of which the glass windows were substituted by polyimide film to ensure low scattering of the device. The shear cell was used to study the relaxation of the interchain orientation of the LCPs. A stack of melt drawn tapes was wrapped in polyimide-tape (kapton). The stack of melt-drawn tapes was heated to 180 °C at a rate of 30 °C min^{-1}, followed by an isothermal period of 10 min. The orientation parameter (S), $\langle P_{2n}(\cos\varphi)\rangle_d$, was calculated from the obtained diffraction patterns via the procedure described by Mitchell and Windle.[24] The azimuthal intensity $I(\varphi)$ at the maximum of the interchain diffraction peak (2θ = 21°) was taken. The orientation parameter $\langle P_{2n}(\cos\varphi)\rangle_d$ was then determined from an average of a Legendre polynomial, weighted against the obtained azimuthal intensity scan using eqs 1−3. In this case, only the second order Legendre polynomial was taken into account, $\langle P_{2n}(\cos\varphi)\rangle_m = -0.5$.

$$S = \langle P_{2n}(\cos\varphi)\rangle_d = \frac{\langle P_{2n}(\cos\varphi)\rangle}{\langle P_{2n}(\cos\varphi)\rangle_m} \quad (1)$$

https://dx.doi.org/10.1021/acs.macromol.9b02689
Macromolecules 2020, 53, 6690−6702

$$\langle P_{2n}(\cos\varphi)\rangle = \frac{\int_0^{\pi/2} I(\theta,\varphi)P_{2n}(\cos\varphi)\sin\varphi\delta\varphi}{\int_0^{\pi/2} I(\theta,\varphi)\sin\varphi\delta\varphi} \quad (2)$$

$$\langle P_{2n}(\cos\varphi)\rangle_m = \frac{(2n)!}{(-1)^n 2^{2n}(n!)^2} = -\frac{1}{2} \text{ for the second term} \quad (3)$$

The obtained orientation parameter reflects the contributions of the distribution of the director orientation throughout the bulk poly domain sample and the contributions of the director on a molecular level.[25] In short, the orientation parameter reflects the degree of anisotropy of the scattering of polymer chains, while assuming that these chains are infinitely long rigid rods. The values of S vary from 0, corresponding to a random chain orientation similar to the orientation of an isotropic liquid, to unity, corresponding to the perfect alignment of the polymer chains along the orientational axis.

RESULTS AND DISCUSSION

Recently, we have demonstrated a method to obtain thermotropic liquid crystalline polymers with a low processing temperature and tunable molecular weight.[21] To recall, a liquid crystalline prepolymer (**LCPP**), with a low molecular weight, is synthesized via a conventional acidolysis polycondensation (Figure 1a). Subsequently, a chain extension reaction with the **LCPP** and a bis(2-oxazoline) derived from isophthalic acid (**IaOx**) is performed in a reactive extrusion process. During the chain extension reaction, the 2-oxazoline moieties of the **IaOx** react with the carboxylic acid end groups of the **LCPP**, thus linking different **LCPP** chains, producing LCPs with increased molar mass (Figure 1b). The resulting molar mass can controlled via the ratio **LCPP**:**IaOx**. All synthesized LCPs can be considered nematic glasses, since no crystallization is observed upon cooling or annealing. The LCPs exhibit a nematic phase above their respective T_g, and the nematic ordering persists upon cooling below T_g. The nematic to isotropic transition could not be observed due to thermal degradation prior to the transition.

The preparation and characterization of the LCPs used in this study is described in detail in our previous work.[21] The effect of the molecular weight on the viscoelastic behavior and mechanical performance is highlighted in Figure 1c,d. The synthesized prepolymer (**LCPP**) and the resulting chain extended LCPs have excellent mechanical properties, in combination with low processing temperatures and tunable viscosity. Therefore, these materials are suitable candidates as the reinforcing phase of sustainable and reprocessable thermoplastic reinforced composites as will be demonstrated in a later section. Composites consisting of a PLLA matrix and four different LCPs, being the liquid crystalline prepolymer (**LCPP**), and three different chain extended LCPs (**CE-2:1**, **CE-3:2**, and **CE-1:1**, names are based on the ratio **LCPP**:**IaOx**), are prepared and analyzed. The molar mass data of the different LCPs is provided in Table 1.

Processing and Blend Morphology Development. The performance of LCP reinforced thermoplastic composites is highly dependent on the LCP morphology which is in turn determined by the viscosity of the respective constituents of the blend and the processing conditions.[13,16,26,27] A fibrillar LCP morphology ensures sufficient surface area to transfer stresses from the matrix to the LCP fibrils, which is a prerequisite for effective reinforcement.[11,14] During the formation of the fibrils, the initially spherical LCP droplets are stretched in a flow field and the LCP chains are oriented.

Table 1. Molar Ratio, Molecular Weight (M_w), and Dispersity ($Đ$) (as Measured by GPC) for the LCPs Used in This Study

material	molar ratio (LCPP:IaOx)	M_w (kg mol^{-1})	$Đ$(−)
LCPP	1:0	6.3	6.0
CE-2:1	2:1	15.3	9.7
CE-3:2	3:2	20.2	11.7
CE-1:1	1:1	40.5	15.6

The LCP-PLA composites are prepared via extrusion, where the LCP phase is dispersed in the PLLA matrix through droplet breakup resulting from the complex shear and extensional flow fields. Next, the sample is injection molded where shear flow combined with cooling can create and preserve the desired fibrillar LCP morphology. For the LCP droplets to break up and to be finely dispersed in the PLA matrix, the droplets need to deform. The capillary number (κ, eq 4), the ratio between the hydrodynamic forces, and the interfacial forces acting on the droplet, must exceed unity for the droplets to stretch. Upon stretching, the diameter of the LCP droplet decreases until a critical value of the capillary number is reached ($\kappa_{crititcal}$) and the increased surface area of the stretched droplet is no longer stabilized by the hydrodynamic forces: the stretched fibril breaks up into smaller drops. Due to the increasing number of droplets formed during this break up process, the number of droplet collisions increases. Colliding drops can then coalesce to form a larger droplet. Given sufficient time, the rate of coalescence and break up will become equal, and an equilibrium morphology is established.

$$\kappa = \frac{\eta_{matrix}\cdot\dot{\gamma}\cdot d}{\nu_{12}} \quad (4)$$

Deformation and breakup of droplets in a matrix are affected by several additional factors. The critical capillary number, as depicted in Figure 2, is dependent on the viscosity ratio (λ, eq 5) and the type of flow (*e.g.*, shear, or extension). For a droplet to effectively stretch in a shear flow field, λ close to unity or lower is required. Higher values of λ gradually lead to less effective deformation of droplets, until at λ = 3.8 the time scale

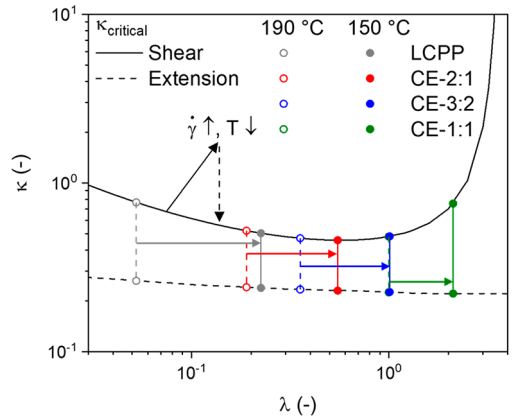

Figure 2. Evolution of the viscosity ratio of different LCP-PLLA blends with temperature. The effect of this transition on the critical capillary number ($\kappa_{critical}$), both in shear and extension, is denoted by the colored points and arrows. The black arrows denote the effect of the change in conditions that occurs upon injection. The viscosity ratio is taken at an oscillation frequency of 137 rad s^{-1}.

https://dx.doi.org/10.1021/acs.macromol.9b02689
Macromolecules 2020, 53, 6690−6702

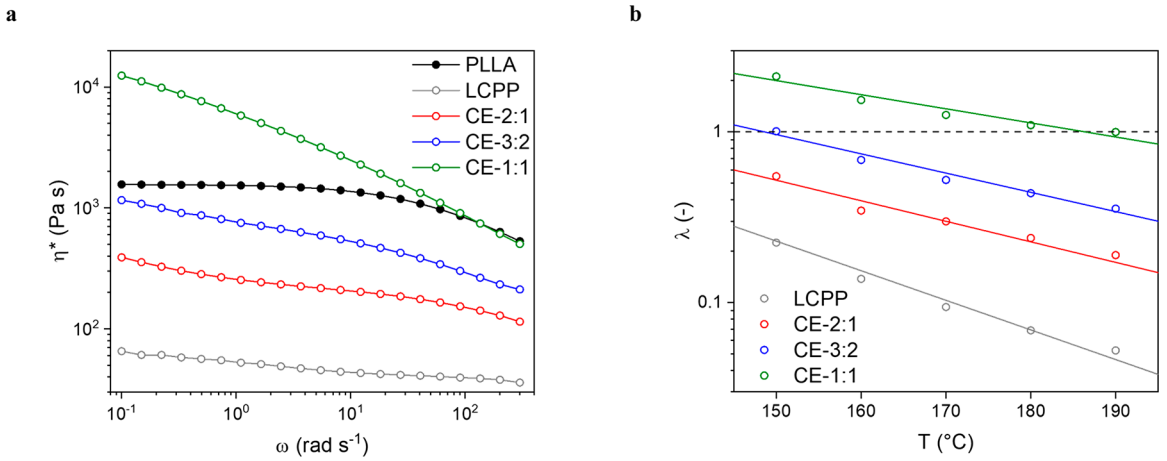

Figure 3. (a) Complex viscosity as a function of oscillation frequency for the PLLA and the different LCPs, measured at 190 °C. (b) Viscosity ratio of the blend consisting of PLLA and the different LCPs as a function of temperature, determined at an oscillation frequency of 137 rad s^{-1}.

for the deformation increases to the extent that the rotational component of the shear flow field rotates the drops instead. Deformation of droplets can be hindered by elastic contributions in the flow behavior of the dispersed phase, due to the increased energy input required for deformation. In contrast, an extensional flow field is effective in deforming droplets regardless of the viscosity ratio of the blend.

$$\lambda = \frac{\eta_{LCP}}{\eta_{\text{matrix}}} \tag{5}$$

Upon injection molding, the molten blend is subjected to a sudden increase in shear rate combined with fast cooling. As a result of these conditions, the capillary number of the LCP droplets increases rapidly and the viscosity ratio of the blend increases as well. Since the droplets can only deform into long fibrils when $\kappa \gg \kappa_{\text{critical}}$ and λ is sufficiently low, the resultant morphology strongly depends on the viscoelastic behavior of both the PLLA matrix and the different LCPs. For example, a low molecular weight LCP is more easily dispersed and stretched compared to an LCP with a higher molecular weight, due to the lower λ of the system. To effectively form a fibrillar morphology with an oriented LCP phase, the viscoelastic behavior and thermal dependency of both phases must be complementary with each other and the chosen processing conditions. For more information on the formation of the morphology of blends, and the behavior of droplets in a matrix, the authors refer to work by Utracki and Shi,[27] our previous works,[16,26] and a clear overview on the subject by Kamal.[28]

The molecular weight control obtained by chain extension of **LCPP** with **IaOx**, and the corresponding control over the viscoelastic behavior (Figure 3a), can effectively be used to generate an LCP phase with the desired viscosity required for processing with the selected PLLA matrix. In more detail, **LCPP**, having the lowest molar mass, hardly shows any shear thinning within the measured frequency range, and a Newtonian plateau is observed over a broad frequency range. At low frequencies, there is an increase in viscosity due to the nematic texture. For the chain-extended LCPs, the shear thinning behavior and the increase in viscosity due to the nematic texture become increasingly more dominant as the molecular weight increases from **CE-2:1** to **CE-1:1**. Correspondingly, the Newtonian plateau ceases to exist for the higher molecular weight LCPs. This transition with increasing molecular weight is commonly observed in LCPs.[29,30] The viscoelastic behavior of the PLLA shows a Newtonian plateau combined with shear thinning behavior at high frequencies. The viscosity of the PLLA exceeds that of all LCPs over the complete measured frequency range, with the exception of **CE-1:1**. In the lower frequency range the viscosity of **CE-1:1** is higher due to the nematic texture; however, in the higher frequency range, which is more relevant for processing, the viscosities of **CE-1:1** and the PLLA are comparable. This indicates that, under extrusion conditions at 190 °C, all of the LCPs have a value of λ close to or below unity (Figure 3b) and can be effectively dispersed in the PLLA matrix selected in this study. Note that all measurements are carried out in the linear viscoelastic regime (Figure S1). This does not correlate directly to the viscoelastic behavior under actual processing conditions that involve unknown flow fields and large deformation, but it does allow a good estimation of the droplet behavior under such conditions.

As the temperature of the molten polymer decreases, the viscosity changes accordingly, influencing the deformation of the LCP droplets. This is specifically relevant for injection molding, as the molten blend is not only deformed but also cooled. The viscosity ratio gradually increases upon cooling for all LCP-PLLA blends (Figure 3b), likely due to the fact that T_g of the LCPs exceeds that of the PLLA. Over the measured temperature range (190−150 °C), the viscosity ratio for the blends with **LCPP** and **CE-2:1** does not exceed unity. For the blend with **CE-3:2**, λ is close to unity over the whole temperature range and only exceeds unity at 150 °C and below. The viscosity ratio for the blend of **CE-1:1** and PLLA increases from unity to two as the temperature decreases to 150 °C. Although deformation of the LCP droplets by the matrix becomes more challenging in this regime and droplets are stretched less efficiently, it can still occur under shear flow, as the limit (λ = 3.8) is not reached. This implies that the LCP droplets can deform into fibrils in all different blends, even during cooling to 150 °C.

The effect of changes in temperature and shear rate, as encountered in injection molding, on the deformability of the LCP droplets are visualized in Figure 2. Upon injection molding, the shear rate increases drastically while the temperature decreases, resulting in an increase in both the viscosity ratio and the capillary number (as depicted by the black arrow in Figure 2). Given that the original viscosity ratio

https://dx.doi.org/10.1021/acs.macromol.9b02689
Macromolecules 2020, 53, 6690−6702

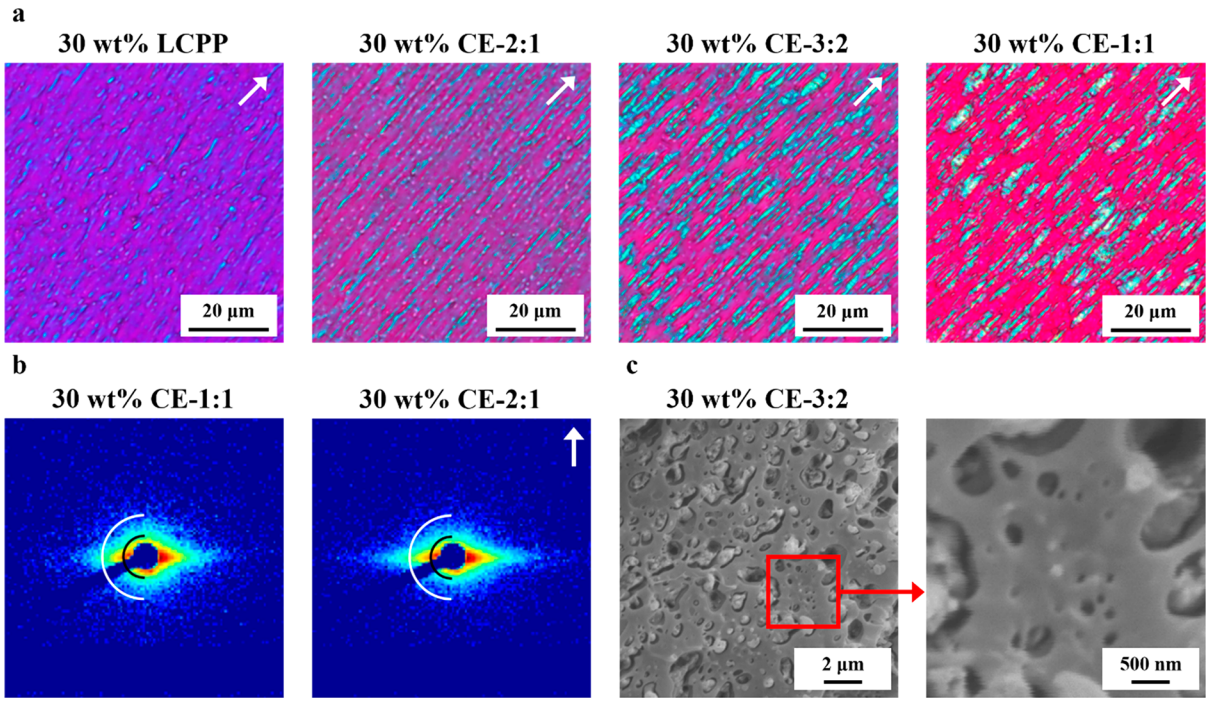

Figure 4. (a) Morphology of injection molded composites containing the different LCPs. The composites were microtomed to slices with a thickness of 1 μm. The images represent the core-region of the sample. The white arrows mark the injection molding direction. (b) SAXS patterns of the injection molded bars containing 30 wt % CE-2:1 and CE-1:1. The white semicircle marks q = 0.125 nm^{-1} (d = 50 nm), whereas the black semicircle marks q = 0.0625 nm^{-1} (d = 100 nm). The white arrows mark the injection molding direction. (c) SEM images showing the LCP particle morphology of an injection-molded composite containing 30 wt % CE-3:2. The left image highlights the distribution of LCP particles with diameters in the micrometer range, whereas the enlarged image on the right highlights a second distribution of particles with sizes in the order of 100 nm.

is not too high (*e.g.*, $\lambda < 2$), these changes result in a state where $\kappa \gg \kappa_{critical}$. This allows the LCP droplets to stretch into fibrils given that the condition $\kappa > \kappa_{critical}$ is met (as depicted by the dotted arrow in Figure 2). The fibrillar morphology is preserved upon further cooling, as both the LCP and the PLLA are quickly cooled below their respective glass transition temperatures.

The morphology of the injection molded bars, containing 30 wt % of the respective LCPs, is shown in Figure 4a. All morphological analysis is performed on the center of the sample, in the core region, as the morphology of the injection molded samples is known to change based on the distance from the mold wall. In all the blends, the LCP is present in the form of finely dispersed fibrils, as was expected from the viscoelastic behavior of the LCPs and PLLA. The uniform coloration of the fibrils viewed by polarized optical microscopy (Figure 4a) indicates a significant degree of interchain orientation of the LCP chains within the fibrils. Clear distinctions can be made with respect to the size and shape of the fibrils of the different LCPs. The **LCPP** fibrils are very thin, with diameters in the order of 600 nm, and appear undulated. Due to its low molecular weight, **LCPP** has the lowest viscosity and proves to be the easiest to disperse in the PLLA matrix resulting in a very fine LCP fibril distribution. However, the low viscosity also results in shorter time scales for breakup of the droplets, likely causing the undulated appearance. Though the fibrils in the **CE-2:**1-PLLA blend are comparable in diameter, they are considerably longer and lack the undulated appearance of the **LCPP** fibrils. Due to the higher viscosity ratio compared to the **LCPP**-PLLA system, the **CE-2:1** fibrils do not break up as quickly as the **LCPP** fibrils, especially when the molten blend is cooled. The fibril morphology in the blend with **CE-3:2** is, although still very fine (fibril diameters in the order of 1−2 μm), considerably more course. In part, this can be explained by the higher viscosity and viscosity ratio. Another contributing factor to the courser morphology is the presence of a physical network in the nematic melt of the chain-extended LCPs with the highest molecular weights (**CE-3:2** and **CE-1:1**). It is known that viscoelastic behavior of the dispersed phase hinders the deformation and breakup of droplets, compared to a purely Newtonian dispersed phase.[31,32] The physical network in the **CE-1:1** and the relatively high viscosity ratio (upon cooling the deformation of the droplets is hindered) of this blend lead to thicker and less stretched fibrils. It should be stated that even for the **CE-1:1** blend, the fibril diameter is around 2−3 μm, which is still considered a very fine dispersion. The observed length of the fibrils appears to be lower than the true length. This discrepancy is attributed to the sample preparation as the fibrils are likely to be at an angle with respect to the cutting plane. This is supported by the microscopy images obtained from thicker slices (Figure S2, slice thickness of 2.5 μm), in which the fibrils are considerably longer. The difference in the morphology of the LCP-PLLA blends highlights the potential of a tunable molecular weight for the use of LCPs in thermoplastic reinforced composites: the viscosity of the LCP can be changed to obtain the optimal fibrillar morphology for a wide range of matrices.

In addition to the LCP fibrils (viewed by optical microscopy), considerably smaller LCP particles (not visible in optical microscopy) appear to be present in all composites. Their presence is confirmed by small-angle X-ray scattering

https://dx.doi.org/10.1021/acs.macromol.9b02689
Macromolecules 2020, 53, 6690−6702

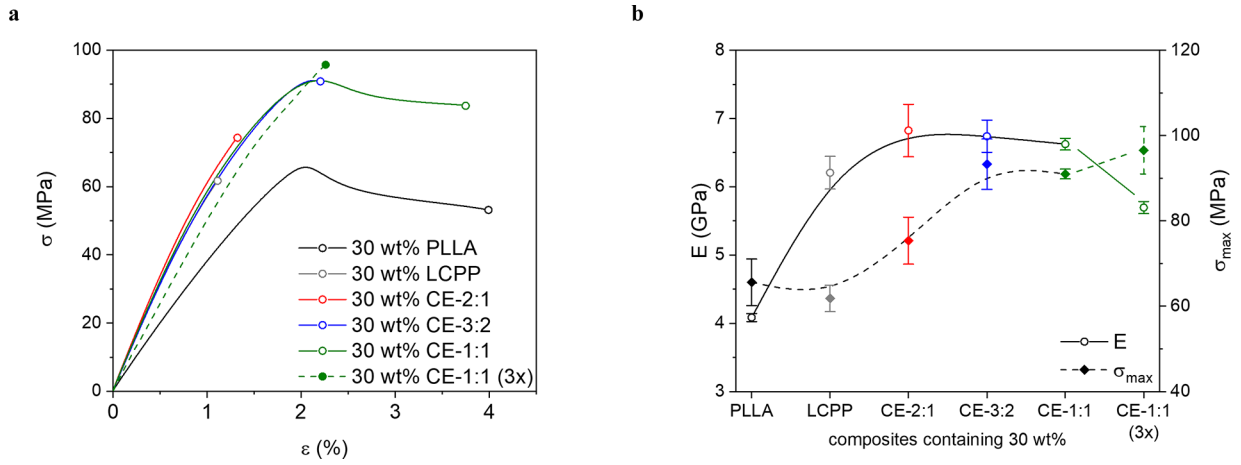

Figure 5. (a) Characteristic stress−strain curves for injection molded bars of pure PLLA, the different LCP-PLLA composites, and the thrice reprocessed CE-1:1-PLLA composite. (b) Young's modulus and stress at break for injection molded bars of pure PLLA, the different LCP-PLLA composites, and the thrice reprocessed CE-1:1-PLLA composite.

(Figure 4b) and scanning electron microscopy (Figure 4c). These particles have a diameter of 100 nm or smaller and are likely to be related to the droplet breakup process. When LCP droplets are stretched to the extent the hydrodynamic forces no longer balance out increasing surface forces, the fibril becomes unstable and breaks up into very small droplets. Considering that the diameter of these droplets is very small, they cannot be deformed by the flow field and can only disappear via coalescence. The small particles are very likely a combination of highly stretched fibrils that are close to instability and the spherical droplets that are the result of breakup of the aforementioned fibrils. In SEM, these particles appear nodular, indicating spherical droplets. The signal in SAXS shows a clear streak corresponding to structures oriented along the flow direction, and the signal is stronger in composites with thinner fibrils (30 wt % **CE-2:1** compared to 30 wt % **CE-1:1**), which indeed indicates the presence of oriented structures periodically spaced along the nanometer range (~100 nm), suggesting that the signal comes from very thin fibrils aligned along the flow direction. Due to the origin of these very fine particles, it is likely that both very small spherical droplets and very thin stretched fibrils are present in the composites.

Injection molded parts typically have a morphology consisting of different layers due the fact that the cooling rate and shear rate vary with the distance to the mold wall.[33,34] Close to the wall the melt experiences very high shear stresses and cooling rates, resulting in a shear layer. Toward the center of the sample, the stresses are lower and the cooling is slower, resulting in a core region with a different morphology. This local variation in conditions causes changes in deformation of the LCP droplets by the PLA matrix, which results in the observation of several layers with different LCP morphologies.[13,35,36] Five distinct layers are observed in all different LCP-PLLA blends, as shown in Figure S3: (1) a quench layer in direct contact with the wall, (2) a shear layer close to the wall, (3) a transition layer a bit further from the wall, (4) a second transition layer, and (5) a core region at the center of the sample. In the shear layer, where the material experiences very high stresses and cooling rates, the LCP is present in form of highly oriented ribbons. The first transition layer characteristically has shorter, irregular fibrils, as the stresses are reduced at this position but the cooling rates remain high. The second transition layer and core layer both have a fibrillar morphology; however, the fibrils in the second transition layer are notably thicker and longer. In both these layers, the cooling rate is relatively low, due to thermal insulation by the other layers, but the higher stresses in the transition layer allows the formation of longer fibrils. Due to the significant LCP loading in the blends (30 wt %), the viscosity of the LCP has an effect on the overall viscosity. The viscosity of the melt is known to affect the thickness of the different layers in injection molding.[33] As the viscosity of the dispersed phase increases with the molecular weight of the LCP, so does the effective viscosity (η_{eff}) of the blend. An overview of the thickness of the four layer for each of the LCP-PLLA composites is shown in Figure S4. The blend containing **LCPP** has the thickest shear layer but relatively thin transition layers. As the viscosity of the LCP increases, the transition layers gradually grow thicker and the shear layer thins. The core decreases gradually in thickness as the LCP viscosity increases up to **CE-1:1**.

Mechanical Performance of Developed Blends. The mechanical properties of the injection molded LCP-PLLA blends are compared to establish whether reinforcement by the LCP phase, as expected from the desired fibrillar morphology, occurs. Indeed, the Young's (E) modulus increases upon the addition of any of the LCPs, while the maximum stress increases for the blends except for the blend containing **LCPP** (Figure 5 and Table 2). The LCP phase has a reinforcing effect in each of the blends; however, it does so more effectively as its molecular weight increases. The most effective reinforcement is achieved in the blends containing **CE-3:2** and **CE-1:1**, resulting in an increase of over 60% in E-modulus and an increase of 40% in maximum stress. The LCPs with lower molecular weights (**LCPP** and **CE-2:1**) are relatively effective in increasing the modulus of the composite, but only the higher molecular weight LCPs (**CE-3:2** and **CE-1:1**) effectively increase the maximum stress. In fiber-reinforced composites, it is often seen that such a trend is related to the morphology, more specifically the fiber length: short fibers improve the E-modulus, but longer fibers are required to increase the stress at break and impact resistance. In the case of these LCP-PLLA composites; however, it is unlikely that the morphology is the only factor, as the LCP is present as finely dispersed, highly stretched fibrils in each of the LCP-PLLA composites. Differences in the interchain orientation parameter

https://dx.doi.org/10.1021/acs.macromol.9b02689
Macromolecules 2020, 53, 6690−6702

Table 2. Mechanical Properties and Orientation Parameter of the PLLA and the LCP-PLLA Composites after Injection Molding[a]

material	E (GPa)	σ_{max} (MPa)	ε_{break} (%)	S_{LCP} (−)
PLLA	4.1 ± 0.06	65.6 ± 5.5	3.3 ± 0.6	–
30 wt % **LCPP**	6.2 ± 0.24	61.8 ± 3.1	1.2 ± 0.1	0.67
30 wt % **CE-2:1**	6.8 ± 0.39	75.4 ± 5.5	1.4 ± 0.1	0.72
30 wt % **CE-3:2**	6.7 ± 0.24	93.3 ± 5.9	2.1 ± 0.4	0.72
30 wt % **CE-1:1**	6.6 ± 0.09	91.0 ± 1.1	3.1 ± 0.6	0.64
30 wt % **CE-1:1** (3x)	5.7 ± 0.09	97.0 ± 5.4	2.2 ± 0.2	0.57
LCPP	7.2 ± 0.14	85 ± 14	1.6 ± 0.33	0.59
CE-2:1	12.5 ± 0.24	164 ± 19	2.2 ± 0.75	0.72
CE-3:2	12.8 ± 0.25	199 ± 16	3.6 ± 0.99	0.72
CE-1:1	12.8 ± 0.17	216 ± 15	4.2 ± 0.96	0.71

[a]The thrice reprocessed **CE-1:1**-PLLA composite is included. The mechanical performance of the pure LCPs is reported for comparison.

(S_{LCP}, Table 2) and the intrinsic mechanical properties of the LCPs have a dominant role on the mechanical response of each composites. As an example, **LCPP**, as a pure LCP, is considerably weaker than the chain-extended LCPs at comparable levels of interchain orientation. The gradual increase in maximum stress of the composites appears to correlate strongly with the stress at break observed for the pure LCP materials. The slight decrease in E-modulus in the blend containing **CE-1:1** compared to **CE-2:1** and **CE-3:2**; however, is expected to be the result of the morphology: due to the relatively high viscosity ratio of the blend, deformation of the LCP droplets is somewhat hindered, resulting in a lower degree of orientation and concomitantly a lower E-modulus of the reinforcing phase.

An improved tensile modulus and tensile strength accomplished by LCP reinforcement is typically accompanied by increased brittleness and thus lower strain at break. This is indeed the case for the composites containing **LCPP** and **CE-2:1**. However, the composites containing **CE-3:2** and **CE-1:1** prove relatively ductile (Figure 3b, Table 2), at least compared to the pure PLLA reference. The **CE-3:2** composite reaches a yield point and subsequently breaks immediately. The **CE-1:1** composites do actually yield and have a strain at break comparable to the pure PLLA: the composite is not only reinforced but also toughened. A very similar trend is found for the pure LCPs, where the higher molecular weight LCPs have a strain at break over 4%. Not only are these relatively ductile reinforced composites interesting from an application perspective but their ductility also provides information on the LCP-PLLA interface. The fact that the stress and strain at break of the LCP-PLLA composites show the same trend as the pure LCPs indicates that strength of the LCP-PLLA interface is high, as the interfacial strength is not expected to vary significantly between the different LCPs. This is confirmed by SEM (Figure 4c), as the LCP fibrils are indeed broken at the fracture surface instead of pulled out. This also implies that the interfacial tension in the molten LCP-PLLA blends is low, which is in agreement with the very low diameter of the LCP fibrils after processing.

In order to mimic recycling and assess the reprocessability of these LCP-PLLA composites, the 30 wt % **CE-1:1** composite was reprocessed three times [sample **CE-1:1** (3×)]. Effective reinforcement is maintained; however, the Young's modulus and strain at break decrease upon reprocessing. This is likely caused by a coarser morphology, with less deformed fibrils and a lower LCP orientation. Due to thermal degradation of the PLLA, the viscosity ratio of the blend gradually increases, resulting in less effective deformation of the LCP in the molten blend.[16] However, overall this is a promising result as significant reinforcement was maintained over three reprocessing cycles. To maintain the mechanical performance upon reprocessing, the use of a higher viscosity PLLA matrix (in combination with **CE-1:1**) or a different LCP (**CE-3:2** with the same PLLA matrix) will be beneficial, as this prevents infeasible viscosity ratios upon reprocessing.[16]

Liquid Crystalline Polymer Relaxation and Its Dependency on the Matrix Viscosity. The degree of interchain orientation of the LCP (S_{LCP}) is one of the key parameters influencing the mechanical performance of the LCP reinforced composites. The glassy nematic nature of the **LCPP** and the chain extended LCPs implies that the LCP will readily relax at temperatures above T_g, resulting in a rapid decrease in interchain orientation. However, in a previous study, we have found that the presence of a physical molecular network structure in chain-extended LCPs limits relaxation as the LCPs retain a significant degree of interchain orientation, even after 10 min at temperatures over a 100 °C above T_g.

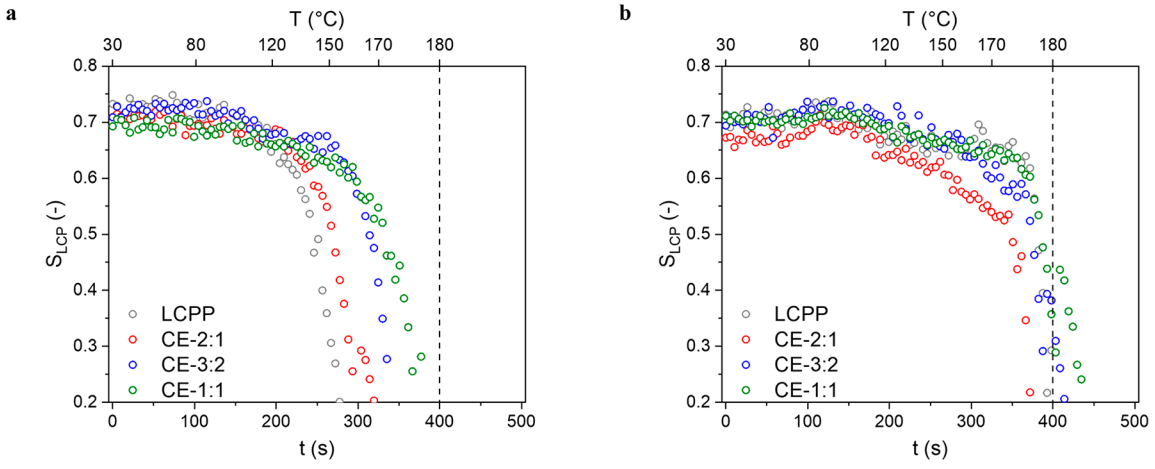

Figure 6. (a) Evolution of the orientation parameter (S_{LCP}) of the different LCPs dispersed in (amorphous) PLA tapes upon heating. (b) Evolution of the orientation parameter (S_{LCP}) of the different LCPs dispersed in (semicrystalline) PLLA tapes upon heating.

https://dx.doi.org/10.1021/acs.macromol.9b02689
Macromolecules 2020, 53, 6690−6702

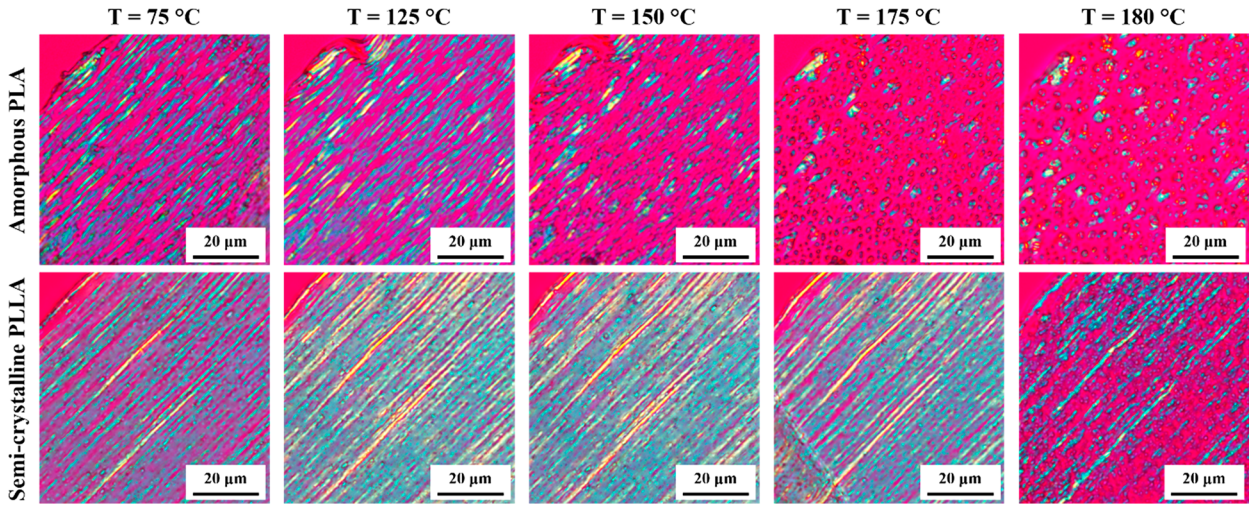

Figure 7. Evolution of the fibrillar morphology of the LCP dispersed in different matrices upon heating: an amorphous PLA matrix (top) and a semicrystalline PLLA matrix (bottom).

This is a highly interesting property of these chain extended LCPs; however, it might not persist in composites as the surface tension provides an additional driving force for relaxation.

Generally, the textural relaxation of nematic LCPs occurs via the annihilation of disclinations: the coalescence of the polydomain texture results in the macroscopic decrease of interchain orientation.[37] Upon deformation, the nematic domains stretch and break up, and relaxation occurs via initial contraction followed by the slower coalescence process. Due to the smaller domains created at higher shear rates, the coalescence is accelerated.[38] In blends the interfacial tension between the dispersed LCP phase, and the PLA matrix phase can play a role and introduce different processes, such as fibril break up, that influence the molecular relaxation of the LCP. The effect of the matrix on the relaxation of the interchain-orientation of **LCPP** and the chain extended LCPs is investigated via wide-angle X-ray diffraction (WAXD). Melt drawn tapes, containing 30 wt % of the respective LCPs, are prepared on a lab-scale spinning setup. Two different poly(lactide) grades were used as the matrix phase: a semicrystalline grade with a low D-isomer content (PLLA), and an amorphous grade with a higher D-isomer content (PLA). The molar mass distribution and viscosity of both grades are very similar (Figure S5). The melt-drawn tapes are wrapped in a polyimide-tape and heated to 180 °C while collecting data at a synchrotron radiation source. The orientation parameter (S_{LCP}) of the dispersed LCP is monitored and shown separately for tapes with the amorphous PLA matrix (Figure 6a) and the semicrystalline PLLA matrix (Figure 6b). The orientation parameter at room temperature was similar for all samples ($S_{LCP} \sim 0.71$), providing a good basis for comparison. In the amorphous matrix, the interchain orientation starts to decrease slowly as the LCPs are heated above their respective T_g's and the relaxation process accelerates as the samples are continuously heated. The observed relaxation rate depends on the viscosity of the LCP, as the chain-extended LCPs with higher molecular weight relax slower. The behavior of the tapes with the PLLA matrix is quite different. Due to the slow crystallization kinetics and high cooling rates applied in the drawing process, the PLLA was initially amorphous. Upon heating the PLLA crystallizes (T = 90−120 °C, t = 100−150 s). This is accompanied by a slight, temporary, increase in the orientation parameter of all the LCPs, likely due to stresses imposed on the LCP fibrils by the shrinking PLLA matrix. Subsequently, the interchain orientation of the LCPs remains constant upon further heating, until the semicrystalline PLLA melts and interchain orientation drops.

The relaxation of the interchain orientation of LCPs in a matrix differs significantly from relaxation of the pure LCP and is highly dependent on the matrix viscosity. When the matrix viscosity remains low upon heating (*e.g.*, amorphous PLA above its T_g, Figure 6a), the decrease in interchain orientation appears not to be governed by the contraction and subsequent coalescence of the polydomain texture, as is observed in the pure LCPs. Instead it appears that the relaxation of the fibrillar morphology is dominant, as the relaxation starts when both the LCP and the matrix are above their T_g. Additionally, there appears to be a strong dependence on the LCP viscosity as the LCP relaxation is delayed for blends having LCP with a higher molecular weight (Figure 6a). However, in this case, the matrix crystallizes upon heating (*e.g.*, PLLA, Figure 6b), relaxation of the fibrillar morphology is not possible, and the LCPs retain a significant degree of orientation until the matrix melts. This is supported by optical microscopy (Figure 7), as microtomed slices of tapes consisting of **CE-1:1** in both the PLA and PLLA matrices are heated, while the changes in morphology are captured. In the amorphous PLA matrix, the fibrils can gradually relax as the temperature increases. In the semicrystalline PLLA matrix, oriented PLLA crystals are formed upon heating, as indicated by the increased birefringence at 125 °C. The crystallized matrix is so rigid that it does not allow relaxation of the fibrils. Only as the crystals are completely molten and no longer stabilize the elongated shape of the fibrils, relaxation to spherical droplets and the concomitant relaxation of the interchain orientation can occur. Until this point, the birefringence of the **CE-1:1** fibrils remains unchanged, indicating that the interchain orientation is maintained upon heating, as is the case for the pure LCPs.

In the absence of a matrix phase, a significant degree of interchain orientation is maintained upon heating, especially as the molecular weight of the LCP increases. In the presence of a matrix, however, additional parameters (*e.g.*, interfacial tension,

https://dx.doi.org/10.1021/acs.macromol.9b02689
Macromolecules 2020, 53, 6690−6702

matrix viscosity, and LCP viscosity) play a significant role. As previously described, relaxation of the interchain orientation of the LCP embedded in a matrix strongly resembles that of the pure LCPs, given that the matrix is either solid or viscous enough to prevent or drastically delay the relaxation of the fibrillar morphology. Therefore, the LCP reinforced tapes with the semicrystalline PLLA matrix are heated to 175 °C, below the full melting temperature of the PLLA crystals, and annealed for 10 min (Figure 8). Under these conditions,

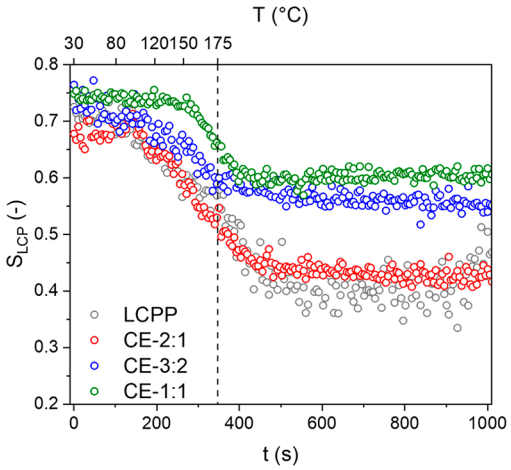

Figure 8. Evolution of the orientation of the different LCPs dispersed in a semicrystalline PLLA matrix upon heating the tapes to 175 °C.

some interchain orientation of the LCPs is maintained, even after annealing. This behavior is similar to that of the pure LCPs and the same trends with respect to the molecular weight of the LCPs are observed: in a low molecular weight LCP (*e.g.*, **LCPP**), the onset of relaxation occurs at a relatively low temperature and the decrease in S_{LCP} is larger, whereas the onset for relaxation for higher molecular weight LCPs (*e.g.*, **CE-1:1**) is at a higher temperature and a larger degree of orientation is retained.

The evolution of the LCP interchain orientation in different tapes and at different annealing temperatures is shown for **CE-2:1** (Figure 9a) and **CE-1:1** (Figure 9b) in order to compare the effect of the different parameters on the relaxation behavior. Compared to the pure LCP, the relaxation of the interchain orientation occurs at lower temperatures in the blends, regardless of whether the matrix phase crystallizes upon heating or not. The extent of the relaxation is also larger in the case the LCP is dispersed in a matrix. The earlier onset of relaxation in LCP-PLLA blends can potentially be explained via the "matrix" viscosity. In the pure LCPs, relaxation of a nematic domain requires mobility in neighboring domains: in a way, the LCP acts as its own "matrix". Due to the lower T_g of PLLA compared to the LCPs, the LCP in the LCP-PLLA tapes experiences a lower matrix viscosity compared to the pure LCP tapes. Initially, there appears to be no influence on the type of PLA that acts as the matrix phase, which fits with the concept that the matrix viscosity determines the onset of relaxation, as the molecular weight and viscosity of both PLA's are similar. At higher temperatures, the crystallites formed in the semicrystalline PLLA prevent relaxation of the LCP's fibrillar morphology and delay the decrease in the interchain orientation with respect to the LCP fibrils in amorphous PLA. The molecular relaxation of the LCP in the semicrystalline matrix resembles that of the pure LCP, governed by contraction of the polydomain texture followed by coalescence, as it shows a similar slow onset and eventually maintains a constant degree of orientation.

In the tapes with a semicrystalline PLLA matrix, the temperature to which the tapes are heated affects the relaxation significantly. As previously seen, melting of the PLLA crystals allows the relaxation of the LCP's fibrillar structure, correspondingly diminishing the degree of orientation. In this case, the tapes are heated to a temperature below the melting temperature of PLLA, a level of orientation of the LCP chains is maintained, and this level depends on the annealing temperature: when annealed at 170 °C both **CE-2:1** and **CE-1:1** retain a higher degree of orientation compared to when the respective tapes are annealed at 175 °C.

Cold-Crystallization of PLLA in the Presence of LCP Fibrils. The effect of the matrix phase on the relaxation of the LCP has been described in detail in previous sections. However, it is known that LCPs can also affect the crystallization behavior of the matrix. For the produced LCP-PLLA tapes, a nucleation effect of the LCP's surface (*e.g.*, some form of epitaxy) is unlikely, as the cold crystallization upon heating of the tapes is not notably accelerated in the presence

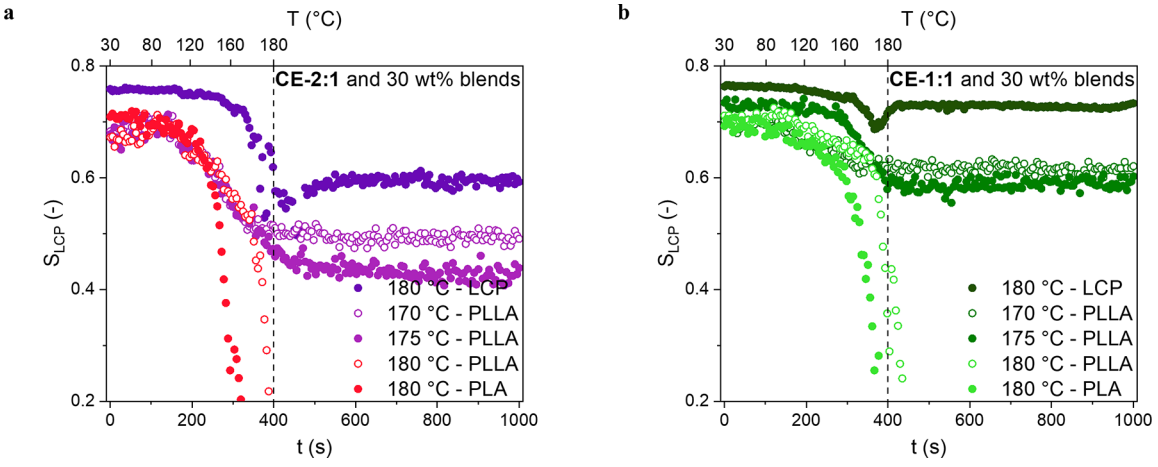

Figure 9. (a) Comparison of the evolution of S_{LCP} for different types of CE-2:1 tapes upon heating. (b) Comparison of the evolution of S_{LCP} for different types of CE-1:1 tapes upon heating.

https://dx.doi.org/10.1021/acs.macromol.9b02689
Macromolecules 2020, 53, 6690−6702

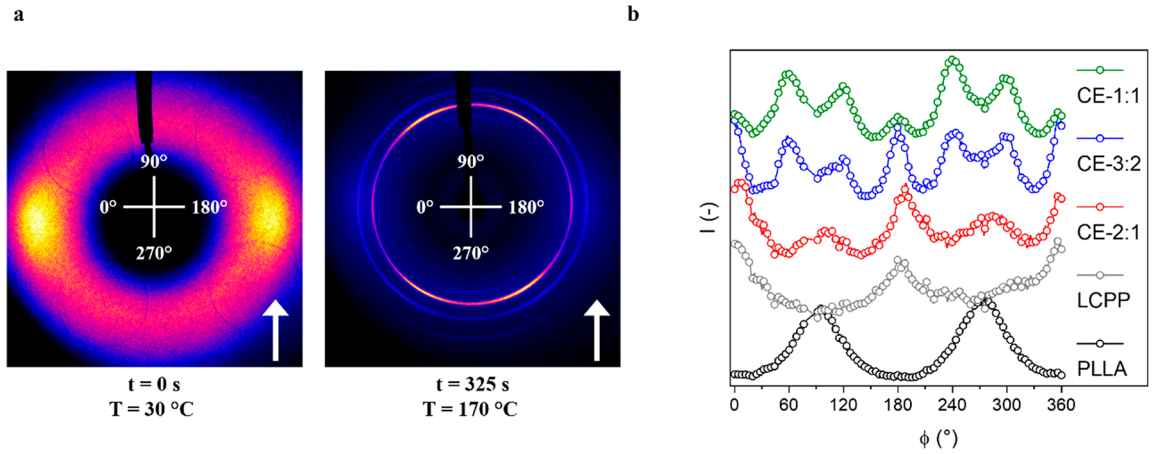

Figure 10. (a) Diffraction patterns of CE-1:1-PLLA tapes at 30 °C and at 170 °C. The white arrows mark the drawing direction, the angles displayed at the center mark the azimuthal angles as displayed in Figure 10b. (b) Normalized azimuthal intensity of the PLLA 110-reflection in the PLLA tape and the different LCP-PLLA tapes, measured at 170 °C. Azimuthal angles of 90° and 270° correspond to the drawing direction.

of the LCPs. In fact, the crystallization of the PLLA is hindered in the presence of any of the LCPs during subsequent cooling, as shown in Figure S6. The PLLA-tapes appear isotropic prior to heating; however, upon crystallization during heating (cold-crystallization), we observe the rise of an interchain diffraction signal with a orientation along the drawing direction (90° and 270°). Due to the small thickness and width of the tape, a confinement effect is expected to facilitate dominant growth of lamellae along the drawing direction.[39,40] However, as shown in Figure 10a, the cold crystallization of the PLLA is affected by the presence of the **CE-1:1** fibrils. Upon heating, the tapes containing LCP fibrils and an apparently isotropic PLLA matrix crystallize and the 110-reflection of the PLLA crystals exhibits a 6-fold symmetry. It stands to reason to assume that the distribution of LCP fibrils limit the previously observed dominant growth of the PLLA lamellae along the drawing direction. Additionally, we consider it likely that the presence of the LCP induces stresses in the PLLA, both during processing and during heating of the tapes. Such (residual) stresses are known to induce the growth of twisted lamellae in materials such as *i*-PP and PLLA,[41−44] which are a plausible explanation for the reflections at 60° and 120° (and correspondingly 240° and 300°). The signals become more dominant in the tapes containing the more viscous LCPs (**CE-3:2** and **CE-1:1**, Figure 10b), since these require more stress to deform and therefore result in more residual stresses. In the LCP-PLLA tapes, a signal arises where the PLLA chains within the crystal are oriented along the drawing direction (0° and 180°), which are more dominant in the tapes containing the lower viscous LCPs (**LCPP** and **CE-2:1**). A full overview of the diffraction patterns of the annealed tapes is displayed in Figure S7.

CONCLUSIONS

We have demonstrated the production of reinforced thermoplastic composites based on several LCPs with different molar masses and PLLA. The morphology of the injection molded composites is evaluated and is found to be in qualitative agreement with predictions based on theory and the viscoelastic behavior of the blend constituents. This highlights not only the enormous influence the morphology and the mechanical properties of the reinforcing phase have on the overall performance of the composites but also the potential benefit of LCPs with tunable molecular weight and viscosity. A fibrillar morphology is obtained via injection molding for all composites, even forming fibrils with submicron diameters in the case of the LCPs with lower molar mass. Though a highly suitable morphology is formed for all the tested LCPs, the mechanical performance of the composites containing LCPs with higher molar mass improved more substantially. This more significant increase is attributed to the intrinsic mechanical performance of these chain-extended LCPs. Compared to the pure PLLA samples, the Young's modulus and stress at break of the injection molded composites containing the high molar mass LCP is increased by 60% and 40%, respectively. Interestingly, this does not result in increased brittleness of the composite, due to a high interfacial strength and the relatively high ductility of the used LCP. The reprocessability of the LCP-PLLA composites is demonstrated.

The relaxation of the interchain orientation of the LCP in a PLA matrix is evaluated in detail. The viscosity of the matrix-phase is found to be the dominant parameter. In blends, the mechanism by which the interchain orientation of the LCP decreases differs from pure LCPs as it is related to the relaxation of the fibrillar LCP morphology. The orientation of the LCP is maintained when the fibrillar LCP morphology remains intact, *e.g.*, when the matrix cold crystallizes upon heating.

The presence of the LCP is found to affect the cold crystallization of the PLLA matrix. Although, no increase in nucleation or crystallization rate is observed, the PLLA crystallites were oriented not only along the draw direction but also at angles of 60° and 90° with respect to the draw direction. The relative intensity of the signal at 60° and 90° to the draw direction increases with the molar mass of the dispersed LCP and are the result of the twisted lamellae formed due to residual stresses. Overall, these findings highlight the importance of viscosity control in thermoplastic blends; control over both the matrix and filler viscosity and their temperature dependency allow for control over particle size, distribution, relaxation, interchain orientation and lamellar morphology, and orientation upon cold-crystallization of the matrix. The resulting composites do not only possess good mechanical properties but are also reprocessable.

https://dx.doi.org/10.1021/acs.macromol.9b02689
Macromolecules 2020, 53, 6690−6702

■ ASSOCIATED CONTENT

Supporting Information

The Supporting Information is available free of charge at https://pubs.acs.org/doi/10.1021/acs.macromol.9b02689.

Evaluation of the linear viscoelastic regime of the LCPs at different temperatures, additional information on fibril morphology of injection molded bars containing 30 wt % of the respective LCPs, layer morphology of injection molded bars containing 30 wt % of the respective LCPs, comparison of the viscoelastic behavior of semicrystalline PLLA and amorphous PLA grades, DSC traces of melt drawn tapes, and diffraction patterns of melt drawn tapes with PLLA (PDF)

■ AUTHOR INFORMATION

Corresponding Authors

Gijs W. de Kort − *Aachen-Maastricht Institute of BioBased Materials (AMIBM), Maastricht University, 6200MD Maastricht, The Netherlands;* orcid.org/0000-0002-6369-1377; Email: gijs.dekort@maastrichtuniversity.nl

Carolus H. R. M. Wilsens − *Aachen-Maastricht Institute of BioBased Materials (AMIBM), Maastricht University, 6200MD Maastricht, The Netherlands; Sabic Technology & Innovation, STC Geleen, 6160AL Geleen, The Netherlands;* orcid.org/0000-0003-3063-9510; Email: karel.wilsens@sabic.com

Authors

Sarah Saidi − *LMOPS, EA 4423, Université de Lorraine, Metz F-57070, France; Netherlands Organisation for Scientific Research (NWO), DUBBLE@ESRF BP CS40220, 38043 Grenoble, France*

Daniel Hermida-Merino − *Netherlands Organisation for Scientific Research (NWO), DUBBLE@ESRF BP CS40220, 38043 Grenoble, France*

Nils Leoné − *Aachen-Maastricht Institute of BioBased Materials (AMIBM), Maastricht University, 6200MD Maastricht, The Netherlands*

Varun Srinivas − *Aachen-Maastricht Institute of BioBased Materials (AMIBM), Maastricht University, 6200MD Maastricht, The Netherlands*

Sanjay Rastogi − *Aachen-Maastricht Institute of BioBased Materials (AMIBM), Maastricht University, 6200MD Maastricht, The Netherlands;* orcid.org/0000-0002-7804-7349

Complete contact information is available at: https://pubs.acs.org/10.1021/acs.macromol.9b02689

Notes

The authors declare no competing financial interest.

■ ACKNOWLEDGMENTS

The research leading to these results has received funding by the H2020 Framework Program of the European Union under Grant N°685614. NWO (Nederlandse Organisatie voor Wetenschappelijk Onderzoek) is acknowledged for providing beam time at the ESRF. The staff of the DUBLLE (Dutch Belgian beamline, ESRF) are acknowledged for supporting the X-ray experiments.

■ REFERENCES

(1) Bakis, C. E.; Bank, L. C.; Brown, V. L.; Cosenza, E.; Davalos, J. F.; Lesko, J. J.; Machida, A.; Rizkalla, S. H.; Triantafillou, T. C. Fiber-Reinforced Polymer Composites for Construction - State-of-the-Art Review. *J. Compos. Constr.* **2002**, *6* (2), 73−87.

(2) Asmatulu, E.; Twomey, J.; Overcash, M. Recycling of Fiber-Reinforced Composites and Direct Structural Composite Recycling Concept. *J. Compos. Mater.* **2014**, *48* (5), 593−608.

(3) Song, Y. S.; Youn, J. R.; Gutowski, T. G. Life Cycle Energy Analysis of Fiber-Reinforced Composites. *Composites, Part A* **2009**, *40* (8), 1257−1265.

(4) Pimenta, S.; Pinho, S. T. Recycling Carbon Fibre Reinforced Polymers for Structural Applications: Technology Review and Market Outlook. *Waste Manage.* **2011**, *31* (2), 378−392.

(5) Eriksson, P. A.; Albertsson, A. C.; Boydell, P.; Prautzsch, G.; Månson, J. A. E. Prediction of Mechanical Properties of Recycled Fiberglass Reinforced Polyamide 66. *Polym. Compos.* **1996**, *17* (6), 830−839.

(6) Kuram, E.; Tasci, E.; Altan, A. I.; Medar, M. M.; Yilmaz, F.; Ozcelik, B. Investigating the Effects of Recycling Number and Injection Parameters on the Mechanical Properties of Glass-Fibre Reinforced Nylon 6 Using Taguchi Method. *Mater. Eng.* **2013**, *49*, 139−150.

(7) Davies, P.; Le Duigou, A.; Pillin, I.; Baley, C.; Bourmaud, A. Effect of Recycling on Mechanical Behaviour of Biocompostable Flax/Poly(l-Lactide) Composites. *Composites, Part A* **2008**, *39* (9), 1471−1478.

(8) Thomason, J. L.; Vlug, M. A.; Schipper, G.; Krikor, H. G. L. T. Influence of Fibre Length and Concentration on the Properties of Glass Fibre-Reinforced Polypropylene: Part 3. Strength and Strain at Failure. *Composites, Part A* **1996**, *27* (11), 1075−1084.

(9) Morin, C.; Loppinet-Serani, A.; Cansell, F.; Aymonier, C. Near- and Supercritical Solvolysis of Carbon Fibre Reinforced Polymers (CFRPs) for Recycling Carbon Fibers as a Valuable Resource: State of the Art. *J. Supercrit. Fluids* **2012**, *66*, 232−240.

(10) Goto, M.; Sasaki, M.; Tokuno, S.; Shibata, K.; Iwaya, T. Recycling of Fiber Reinforced Plastics Using Depolymerization by Solvothermal Reaction with Catalyst. *J. Mater. Sci.* **2008**, *43* (7), 2452−2456.

(11) Bassett, B. R.; Yee, A. F. A Method of Forming Composite Structures Usingin Situ-Formed Liquid Crystal Polymer Fibers in a Thermoplastic Matrix. *Polym. Compos.* **1990**, *11* (1), 10−18.

(12) Wang, H.; Lee, K. W.; Chung, T. S.; Jaffe, M. Rheology, Morphology and Properties of LCP/Nylon 66 Composite Fibers. *Polym. Compos.* **2000**, *21* (1), 114−123.

(13) Kiss, G. In Situ Composites: Blends of Isotropic Polymers and Thermotropic Liquid Crystalline Polymers. *Polym. Eng. Sci.* **1987**, *27* (6), 410−423.

(14) Blizard, K. G.; Federici, C.; Federico, O.; Chapoy, L. L. The Morphology of Extruded Blends Containing a Thermotropic Liquid Crystalline Polymer. *Polym. Eng. Sci.* **1990**, *30* (22), 1442−1453.

(15) Silverstein, M. S.; Hiltner, A.; Baer, E. Hierarchical Structure in LCP/PET Blends. *J. Appl. Polym. Sci.* **1991**, *43* (1), 157−173.

(16) de Kort, G. W.; Bouvrie, L.; Rastogi, S.; Wilsens, C. H. R. M. Thermoplastic PLA-LCP Composites: A Route towards Sustainable, Reprocessable, and Recyclable Reinforced Materials. *ACS Sustainable Chem. Eng.* **2020**, *8*, 624−631.

(17) Chung, T.-S. The Recent Developments of Thermotropic Liquid Crystalline Polymers. *Polym. Eng. Sci.* **1986**, *26* (13), 901−919.

(18) Han, H.; Bhowmik, P. K. Wholly Aromatic Liquid-Crystalline Polyesters. *Prog. Polym. Sci.* **1997**, *22* (7), 1431−1502.

(19) Heino, M. T.; Hietaoja, P. T.; Vainio, T. P.; Seppälä, J. V. Effect of Viscosity Ratio and Processing Conditions on the Morphology of Blends of Liquid Crystalline Polymer and Polypropylene. *J. Appl. Polym. Sci.* **1994**, *51* (2), 259−270.

(20) Tan, L. P.; Yue, C. Y.; Tam, K. C.; Lam, Y. C.; Hu, X. Effects of Shear Rate, Viscosity Ratio and Liquid Crystalline Polymer Content on Morphological and Mechanical Properties of Polycarbonate and LCP Blends. *Polym. Int.* **2002**, *51* (5), 398−405.

(21) de Kort, G. W. *Thermotropic Polyesters and Polylactide: A Route to Sustainable and Reprocessable Reinforced Composites*, PhD Thesis, Maastricht University, 2020.
(22) Bras, W.; Dolbnya, I. P.; Detollenaere, D.; Van Tol, R.; Malfois, M.; Greaves, G. N.; Ryan, A. J.; Heeley, E. Recent Experiments on a Combined Small-Angle/Wide-Angle X-Ray Scattering Beam Line at the ESRF. *J. Appl. Crystallogr.* **2003**, *36*, 791−794.
(23) Portale, G.; Cavallo, D.; Alfonso, G. C.; Hermida-Merino, D.; Van Drongelen, M.; Balzano, L.; Peters, G. W. M.; Goossens, J. G. P.; Bras, W. Polymer Crystallization Studies under Processing-Relevant Conditions at the SAXS/WAXS DUBBLE Beamline at the ESRF. *J. Appl. Crystallogr.* **2013**, *46* (6), 1681−1689.
(24) Mitchell, G. R.; Windle, A. H. Orientation in Liquid Crystal Polymers. In *Developments in crystalline polymers*; Basset, D. C., Ed.; Elsevier Applied Science: London, UK, 1988, DOI: 10.1007/978-94-009-1341-7_3.
(25) Ugaz, V. M.; Burghardt, W. R.; Zhou, W.; Kornfield, J. A. Transient Molecular Orientation and Rheology in Flow Aligning Thermotropic Liquid Crystalline Polymers. *J. Rheol. (Melville, NY, U. S.)* **2001**, *45* (5), 1029−1063.
(26) de Kort, G. W.; Rastogi, S.; Wilsens, C. H. R. M. Controlling Processing, Morphology, and Mechanical Performance in Blends of Polylactide and Thermotropic Polyesters. *Macromolecules* **2019**, *52*, 6005−6017.
(27) Shi, H.; Utracki, L. A. Development of Polymer Blend Morphology During Compounding in a Twin-Screw Extruder. Part II: Theoretical Derivations. *Polym. Eng. Sci.* **1992**, *32* (24), 1834−1845.
(28) Kamal, M. R.; Utracki, L. A.; Mirzadeh, A. Rheology of Polymer Alloys and Blends. In *Polymer Blends Handbook*, Vol. 2; Utracki, L. A., Wilkie, C., Eds.; Spring Netherlands: Dordrecht, 2014; pp 726−853, DOI: 10.1007/978-94-007-6064-6.
(29) Sigillo, I.; Grizzuti, N. The Effect of Molecular Weight on the Steady Shear Rheology of Lyotropic Solutions. A Phenomenological Study. *J. Rheol.* **1994**, *38*, 589−599.
(30) Somma, E.; Nobile, M. R. The Linear Viscoelastic Behavior of a Series of Molecular Weights of the Thermotropic Main-Chain Liquid Crystal Polymers HBA/HNA 73/27. *J. Rheol. (Melville, NY, U. S.)* **2004**, *48* (6), 1407−1423.
(31) de Bruijn, R. A. *Deformation and Breakup of Drops in Simple Shear Flows*; Eindhoven University of Technology, 1989, DOI: 10.6100/IR318702.
(32) Kernick, W. a.; Wagner, N. J. The Role of Liquid-Crystalline Polymer Rheology on the Evolving Morphology of Immiscible Blends Containing Liquid-Crystalline Polymers. *J. Rheol. (Melville, NY, U. S.)* **1999**, *43* (3), 521.
(33) Kantz, M. R. The Effects of Melt Processing Variables on the Morphology and Properties of Injection Molded Polypropylene. *Int. J. Polym. Mater.* **1974**, *3* (3), 245−258.
(34) Roozemond, P. C.; Van Drongelen, M.; Ma, Z.; Spoelstra, A. B.; Hermida-Merino, D.; Peters, G. W. M. Self-Regulation in Flow-Induced Structure Formation of Polypropylene. *Macromol. Rapid Commun.* **2015**, *36* (4), 385−390.
(35) Li, Z. M.; Yang, W.; Yang, S.; Huang, R.; Yang, M. B. Morphology-Tensile Behavior Relationship in Injection Molded Poly(Ethylene Terephthalate)/Polyethylene and Polycarbonate/Polyethylene Blends (I): Part I Skin-Core Structure. *J. Mater. Sci.* **2004**, *39* (2), 413−431.
(36) Turcott, E.; Nguyen, K. T.; Garcia-Rejon, A. Microstructure Development during the Injection Molding of PET/LCP Blends. *Polym. Eng. Sci.* **2001**, *41* (4), 603−617.
(37) Hsiao, B. S.; Stein, R. S.; Deutscher, K.; Winter, H. H. Optical Anisotropy of a Thermotropic Liquid-crystalline Polymer in Transient Shear. *J. Polym. Sci., Part B: Polym. Phys.* **1990**, *28* (9), 1571−1588.
(38) de Kort, G. W.; Leoné, N.; Stellamanns, E.; Auhl, D.; Wilsens, C. H. R. M.; Rastogi, S. Effect of Shear Rate on the Orientation and Relaxation of a Vanillic Acid Based Liquid Crystalline Polymer. *Polymers (Basel, Switz.)* **2018**, *10* (9), 935.
(39) Woo, E. M.; Lugito, G.; Tsai, J. H. Effects of Top Confinement and Diluents on Morphology in Crystallization of Poly(l -Lactic Acid) Interacting with Poly(Ethylene Oxide). *J. Polym. Sci., Part B: Polym. Phys.* **2015**, *53* (16), 1160−1170.
(40) Fischer, F. S. U.; Tremel, K.; Sommer, M.; Crossland, E. J. C.; Ludwigs, S. Directed Crystallization of Poly(3-Hexylthiophene) in Micrometre Channels under Confinement and in Electric Fields. *Nanoscale* **2012**, *4* (6), 2138−2144.
(41) Lohmeijer, P. J. A.; Goossens, J. G. P.; Peters, G. W. M. Quiescent Crystallization of Poly(Lactic Acid) Studied by Optical Microscopy and Light-Scattering Techniques. *J. Appl. Polym. Sci.* **2017**, *134* (10), 2−10.
(42) Lotz, B.; Cheng, S. Z. D. A Critical Assessment of Unbalanced Surface Stresses as the Mechanical Origin of Twisting and Scrolling of Polymer Crystals. *Polymer* **2005**, *46* (3), 577−610.
(43) Assouline, E.; Wachtel, E.; Grigull, S.; Lustiger, A.; Wagner, H. D.; Marom, G. Lamellar Twisting in α Isotactic Polypropylene Transcrystallinity Investigated by Synchrotron Microbeam X-Ray Diffraction. *Polymer* **2001**, *42* (14), 6231−6237.
(44) Maillard, D.; Prud'homme, R. E. Crystallization of Ultrathin Films of Polylactides: From Chain Chirality to Lamella Curvature and Twisting. *Macromolecules* **2008**, *41* (5), 1705−1712.